Journal of Nuclear Medicine, published on September 27, 2019 as doi:10.2967/jnumed.119.230961

Total-body PET and highly stable chelators together enable meaningful ^{89}Zr-antibody-PET studies up to 30 days post-injection

Eric Berg[1], Herman Gill[2], Jan Marik[2], Annie Ogasawara[2], Simon Williams[2], Guus van Dongen[3], Daniëlle Vugts[3], Simon R. Cherry[1,4], and Alice F. Tarantal[5]

[1]Department of Biomedical Engineering, University of California, Davis, Davis, California, USA

[2]Department of Biomedical Imaging, Genentech Inc., South San Francisco, California

[3]Department of Radiology and Nuclear Medicine, Amsterdam UMC, VU University, De Boelelaan 1117, 1081HV, Amsterdam, The Netherlands

[4]Department of Radiology, University of California, Davis, School of Medicine

[5]Departments of Pediatrics and Cell Biology and Human Anatomy, School of Medicine, and California National Primate Research Center, University of California, Davis

Corresponding author and first author: Eric Berg, 451 E. Health Sciences Drive, Davis, CA 95616; eberg@ucdavis.edu; (530) 752-0626.

Disclaimer: none.

Word count: 5960

Financial Support: We acknowledge support from NIH R35-CA197608 and P51-OD011107.

Running title: 30-day ^{89}Zr-antibody-PET

ABSTRACT

Rationale: The use of ^{89}Zr-antibody-PET imaging to measure antibody biodistribution and tissue pharmacokinetics is well established, but current PET systems lack the sensitivity needed to study ^{89}Zr-labeled antibodies beyond two to three isotope half-lives (7-10 days), after which poor signal-to-noise is problematic. However, studies across many weeks are desirable to better match antibody circulation half-life in human and nonhuman primates. These studies investigated the technical feasibility of using the primate mini-EXPLORER PET scanner, making use of its high sensitivity and 45 cm axial field-of-view (FOV), for total-body imaging of ^{89}Zr-labeled antibodies in rhesus monkeys up to 30-days post-injection.

Methods: A humanized monoclonal IgG antibody against the herpes simplex viral protein gD was radiolabeled with ^{89}Zr via one of four chelator-linker combinations (DFO-Bz-NCS, DFO-squaramide, DFO*-Bz-NCS, and DFO*-squaramide). The pharmacokinetics associated with these four chelator-linker combinations were compared in 12 healthy young male rhesus monkeys (~1-2 years of age, ~3±1 kg). Each animal was initially injected intravenously with unlabeled antibody (10 mg/kg providing therapeutic-level antibody concentrations; right), immediately followed by ~40 MBq of one of the ^{89}Zr-labeled antibodies injected intravenously at a contralateral site (left). All animals were imaged six times over a period of 30 days, with an initial 60-minute dynamic scan on day 0 (day of injection), followed by static scans of 30-45 minutes on approximately days 3, 7, 14, 21, and 30, with all acquired using a single bed position and images reconstructed using a time-of-flight listmode OSEM algorithm. Activity concentrations in various organs were extracted from the PET images using manually defined regions-of-interest (ROIs).

Results: Excellent image quality was obtained, capturing the initial distribution phase in the whole-body scan, later time points showed residual ^{89}Zr mainly in the liver. Even at 30 days post-

injection, representing approximately 9 half-lives of ^{89}Zr and with a total residual activity in the animal of only 20-40 kBq, the image quality was sufficient to readily identify activity in the liver, kidneys, and bone joints. Significant differences were noted in late time-point liver uptake, bone uptake, and whole-body clearance between chelator-linker types, while little variation (±10%) was observed within each type.

Conclusions: These studies demonstrate the ability to image ^{89}Zr radiolabeled antibodies up to 30 days post-injection while maintaining satisfactory image quality provided by the primate mini-EXPLORER with high sensitivity and long axial FOV. Quantification demonstrated potentially important differences in the behavior of the four chelators, which supports further investigation.

Key Words: Positron emission tomography, immuno-PET, quantification, total-body imaging, rhesus monkey.

INTRODUCTION

Extending human and nonhuman primate positron emission tomography (PET) studies beyond 7 to 10 days post-injection at an acceptable radiation exposure is currently impractical even when using a positron-emitting isotope with an appropriately long half-life such as zirconium-89 (^{89}Zr). ^{89}Zr is the positron emitter of choice for PET imaging of slow kinetic drugs like monoclonal antibodies, and for this purpose ^{89}Zr has to be stably coupled to the antibody via a chelate. Beyond two to three physical half-lives, however, most contemporary commercial scanners are not sufficiently sensitive to collect the necessary coincidence events from the residual ^{89}Zr in the subject to reconstruct images with high signal-to-noise for accurate image interpretation and quantification. While longer scan durations can compensate for decay by collecting more coincidence events, this quickly becomes prohibitive in studies that require sedation or in situations where scan duration is limited by patient comfort, motion, and clinical demands. Therefore, the physical ability to acquire images at later time-points depends primarily on the development of PET scanners with significantly higher sensitivity than those currently available. Once developed, executing biologically meaningful late time-point studies on newly developed PET scanners will depend on the availability of radiotracer molecules such as ^{89}Zr-chelates that maintain their integrity in the body over the multi-week timescale of the study. The investigations described herein illustrates the successful combination of a new total-body PET scanner and novel chelator moieties for ^{89}Zr.

There have been several recent developments in high sensitivity PET systems that are suitable for human and nonhuman primate imaging (*1-4*). In these scanners, substantial sensitivity gains have been achieved by extending the scanner's axial length up to ~2 meters for a human imaging system, and to ~50 cm in the preclinical systems. In this study, we have utilized the primate mini-EXPLORER PET system, a 45 cm long system with National Electrical Manufacturers

Association (NEMA) NU-2 sensitivity of ~50 kcps/MBq which is capable of imaging the entire body of young rhesus monkeys in a single bed position (*1,5*).

PET provides a unique methodology to quantitatively image the biodistribution and kinetics associated with a wide range of molecules *in vivo*, from metabolites to nanoparticles. An increasingly common application is the imaging of radiolabeled antibodies ("antibody-PET"), now an established technique to gain understanding of the behavior of antibodies and their target antigens non-invasively, and to inform, for example, early readouts of the efficacy of novel antibody-based immunotherapies (*6-8*). Since the terminal half-life of therapeutic antibodies in humans is commonly on the order of one to several weeks, the desired imaging time-points can extend over the same time scale to fully determine the fate of the tracer antibodies. In addition to antibodies, other emerging applications that rely on late time-point PET acquisition include imaging the biodistribution of transplanted stem/progenitor cells, chimeric antigen receptor T cells (CAR-T cells) (*9,10*), and radiolabeled nanoparticles (*11,12*). For stem/progenitor cell applications, imaging time-points can be up to two to five weeks post-injection in order to efficiently capture the early biodistribution of the cells that is critically important in evaluating cell trafficking, engraftment, safety, and outcomes over time.

Extending the duration of PET studies beyond 7 to 10 days after the delivery of a radiolabeled imaging agent does present some challenges. First is the need for a positron emitting isotope with a sufficiently long radioactive half-life that is well matched to the biological half-life and uptake time of the imaging agent. Several radioisotopes have been investigated for long-duration PET studies, including copper-64 (^{64}Cu) and iodine-124 (^{124}I), although ^{89}Zr best fulfills many of the desired properties with its 3.27-day half-life. In addition, other favorable physical properties include minimal contamination from the 909 keV prompt gamma photon within the 511 keV PET

energy window, and superior spatial resolution compared to many other positron-emitting isotopes as a result of the relatively low excess decay energy (mean energy of 396 keV). Chemically, the facile incorporation of ^{89}Zr by chelation and the residualizing behavior of ^{89}Zr is often preferred to the covalent labeling reactions and non-residualizing behavior of ^{124}I. As such, ^{89}Zr is now often used to characterize the *in vivo* behavior of slow kinetic molecules by PET, including antibodies and nanobodies (*13-15*).

A challenge associated with the use of ^{89}Zr in studies at late time-points lies in minimizing the release of osteophilic ^{89}Zr ions or low molecular weight catabolites from the imaging agent (i.e., antibody, cell, nanoparticle). Progressively liberated ^{89}Zr catabolites, potentially free $^{89}Zr^{4+}$, have often been observed to accumulate irreversibly in mineralized bone, especially at sites of active bone remodeling such as the joints, which can complicate image interpretation (*16*). These observations are most dominant in preclinical PET studies, with less bone signal observed in clinical studies in general.

Several chelators have been investigated for use in ^{89}Zr-PET studies (*17*), but desferrioxamine B (DFO) remains the most widely adopted. DFO is available commercially with either of two lysine-reactive bifunctional linkers, benzyl isothiocyanate-DFO (DFO-Bz-NCS) or tetrafluorophenyl-N-succinyl-DFO (*18,19*), and has been applied in a variety of ^{89}Zr-PET applications, including human clinical studies (*20,21*). However, *in vivo* PET imaging studies with ^{89}Zr-DFO suggest less than ideal stability beyond approximately three days (*14*). This finding is a consequence of the hexadentate binding complex provided by DFO that is not ideally matched to $^{89}Zr^{4+}$, which prefers the formation of octadentate binding that occupy all available coordination sites of $^{89}Zr^{4+}$. An octadentate variant of DFO, desferrioxamine* (DFO*), was recently developed through the addition of a fourth hydroxamate unit to the chelator (*22,23*). *In vivo* studies in mice

with ^{89}Zr-DFO*-antibodies have demonstrated reduced ^{89}Zr signal in the bone and liver. A potential alternative route to achieve octadentate binding of $^{89}Zr^{4+}$ is through the linker. A new linker, employing a squaramide moiety (*24*), was recently developed on the premise of using a linker that contributes oxygen molecules to the DFO chelator in order to achieve octadentate ^{89}Zr binding. Indeed, DFO-squaramide showed promising *in vivo* results in ^{89}Zr-PET studies with mice. However, a robust comparison of the *in vivo* pharmacokinetics associated with the various ^{89}Zr chelator-linker combinations that are most often used clinically is lacking, and therefore represents a critically needed step towards enabling long-duration ^{89}Zr-PET studies.

The aim of this study was two-fold. The primary goal was to demonstrate the feasibility of extending nonhuman primate ^{89}Zr PET studies to 30-days post-injection by making use of the high sensitivity primate mini-EXPLORER total-body PET system. In addition, we used the late time point imaging capabilities of EXPLORER to quantify the pharmacokinetics associated with four ^{89}Zr chelator-linker combinations based on DFO or DFO* chelators and Bz-NCS or squaramide linkers. We also initiated studies to begin to examine their suitability for long-duration PET studies by assessing pharmacokinetics and the image signal at the joints as an indicator of osteophilic catabolite formation.

MATERIALS AND METHODS

Chelator-Linkers, Antibodies, and Radiolabeling

Four ^{89}Zr chelator-linker moieties were compared: (1) DFO-Bz-NCS, (2) DFO*-Bz-NCS, (3) DFO-squaramide, and (4) DFO*-squaramide (chemical structures are provided in Supplemental Fig. 1). Common solvents and chemicals were purchased from Aldrich (Milwaukee, WI) or VWR International (Radnor, PA) if not stated otherwise. DFO-Bz-NCS was purchased from Macrocyclics (Plano, TX). DFO-squaramide was prepared according the procedure published Rudd et al. (*24*). The DFO* was prepared by the procedure described by Patra et al. (*23*). DFO*-

Bz-NCS was synthesized as described by Vugts et al. (*22*). Anti-gD antibody (specific to glycoprotein D on the herpes simplex virus) was prepared at Genentech, Inc. ^{1}H NMR spectra were acquired on a Bruker Avance II 400 spectrometer at 298 K and the chemical shifts are reported in ppm relative to TMS.

The following systems were used to analyze and purify the products: System A (Analytical LC-MS): Waters Acquity UPLC running at 0.7 mL/min. Column: Acquity UPLC BEH C18 1.7 μm 2.1 × 30 mm. Mobile phase A: water with 0.1% formic acid, B: acetonitrile with 0.1% formic acid, linear gradient 5-95% B in 2 min. The system was equipped with Acquity PDA and Acquity SQ detectors. System B (Preparative HPLC): Interchim PuriFlash pump running at 60 mL/min. Column Phenomenex Gemini-NX 10μ C18 110A AX 100 × 30.00 mm. Mobile phase A: water with 0.1 formic acid, B: acetonitrile. Linear gradient 5-50% B in 10 min. System C (size-exclusion HPLC): Agilent UPLC with an in-line diode array detector and radiation detector (Eckert & Ziegler, Berlin, Germany). Column: TSKgel UP-SW3000, 4.6 × 300 mm (Tosoh Bioscience, King of Prussia, PA, USA). Mobile phase: 150 mM sodium phosphate, 250 mM sodium chloride, 12% isopropanol, pH7.0. Flow rate: 0.26 mL/min.

The synthesis of DFO*-squaramide was performed using the following methodology: DFO* hydrochloride (40 mg, 0.05 mmol) and *N,N*-diisopropylethylamine (9 μL, 0.05 mmol) were mixed in ethanol (3 mL) and heated to 50 °C for 30 min. A solution of diethylsquaramide (25 μL, 0.150 mmol) in ethanol (1.5 mL) was added and pH was adjusted to 8 by *N,N*-diisopropylethylamine. The suspension was stirred at 50 °C for 3 hours. The solvent was removed at reduced pressure and the residue was dissolved in dimethylsulfoxide (2 mL). The solution was injected to preparative HPLC system B and collected fractions were evaporated to dryness. Since NMR analysis of the product revealed presence of squaramide the obtained white solid was washed with acetone to

remove the contamination and dried at reduced pressure to provide DFO*-squaramide as white solid 17 mg (39%). LCMS found m/z 885.4 (calc. for $C_{40}H_{68}N_8O_{14}$ 884.49 Da); purity 96% (UV 254 nm). ^{1}H NMR (400 MHz, DMSO-d6) δ 9.61 (m , 4H), 8.77 (s, 1H), 8.57 (s, 1H), 7.75 (m, 4H), 4.65 (m, 3H), 3.45 (m, 8H), 3.00 (m, 6H), 2.67 (m, 1H), 2.57 (m, 4H), 2.35-2.30 (m, 1H), 2.27 (m, 6H), 1.96 (s, 3H), 1.57-1.43 (m, 10H), 1.37 (m, 8H), 1.22 (m, 8H).

The conjugation of DFO-Bz-NCS and DFO*-Bz-NCS to anti-gD was performed consistent with Vosjan et al. (*25*) and Vugts et al. (*22*). The conjugation of DFO-squaramide and DFO*-squaramide to anti-gD was performed consistent with the method described by Rudd et al. (*24*). The antibodies were prepared with a conjugate to antibody ratio of 1.0-2.0 and a concentration range of 3.7-8.3 mg/mL in succinate formulation buffer (10 mM sodium succinate, 240 mM sucrose, 0.02% polysorbate-20, pH 5.5).

Chelation of ^{89}Zr to each DFO variant was performed consistent with Vosjan et al. (*25*). The antibodies were prepared at a radioactive concentration range of 47-62 MBq/mL and a protein concentration range of 0.80-1.12 mg/mL in the aforementioned succinate formulation buffer. Specific activities at the end of synthesis ranged from 46-77 MBq/mg (DFO-Bz-NCS: 72 MBq/mg; DFO*-Bz-NCS: 58 MBq/mg; DFO-squaramide: 77 MBq/mg; DFO*-squaramide: 46 MBq/mg).

The purity of the ^{89}Zr-labeled DFO variants of anti-gD was measured by system C (Supplemental Fig. 2). Radiolabeling was performed at Genentech South San Francisco and at several time-points up to seven days post-synthesis QC measurements were done. However, it should be noted that the ^{89}Zr-antibody samples used for the imaging studies at UC Davis, although from the same batch as the samples used for QC measurements, were stored separately and the QC sample did not undergo transport to UC Davis.

Rhesus Monkey Cohorts

The pharmacokinetics associated with the four ^{89}Zr chelator-linker combinations were evaluated in 12 indoor-housed healthy male rhesus monkeys (Table 1). An N of three were used for each chelator-linker type. All animal procedures were performed at the California National Primate Research Center and conformed to the requirements of the Animal Welfare Act with protocols approved by the Institutional Animal Care and Use Committee at the University of California, Davis prior to implementation.

Imaging Studies

On study day 0 (day of injection) for each chelator-linker type, the N of three per group were injected intravenously with approximately 40 MBq (min. 36 MBq; max. 47 MBq) of ^{89}Zr-labeled antibody in the left brachial artery (second injection), along with an additional mass dose (10 mg/kg) of unlabeled antibodies injected intravenously in the right brachial artery (first injection). The three animals per group were all completed in sequence on the same day. Each animal was placed on the scan bed designed for the primate mini-EXPLORER scanner, carefully positioned, and imaged individually six times over 30 days. The imaging time points included the day of injection (day 0) then approximately day 3, 7, 14, 21, and 30, with scan durations of 60 minutes for day 0, 45 minutes for day 30, and 30 minutes for all intermediate time-points. The day 0 PET acquisition was initiated approximately two minutes following injection. Dynamic image acquisition using six 10-minute frames was included for the day 0 scans.

All PET studies were conducted using the primate mini-EXPLORER long axial field-of-view (FOV) system (*1*). This system has a 45 cm axial FOV, 43.5 cm bore diameter, a total NEMA NU-2 sensitivity of 50.2 kcps/MBq, and an isotropic spatial resolution of approximately 3 mm at the center of the FOV. All PET scans were acquired with a single bed position and listmode data acquisition. Immediately following each PET acquisition, a whole-body computed tomography

(CT) image was acquired on a GE Discovery® 610 in the same imaging suite, and co-registered to the PET image. The scan bed was used to carefully move each rhesus monkey between scanners to facilitate accurate image registration and without any change in positioning.

Venous blood samples were obtained from each animal at all imaging time-points immediately following the CT acquisition. Antibody concentration in the blood samples was quantified via enzyme-linked immunosorbent assay (ELISA).

Image Reconstruction and Quantification

Images were reconstructed using an in-house developed listmode time-of-flight ordered subsets estimation maximization (TOF-OSEM) algorithm, including corrections for attenuation, dead-time, random coincidences, radionuclide decay, and voxel calibration factor to units of kBq/cc. The 511 keV attenuation factors were derived from the co-registered CT image using bi-linear scaling (*26*). No algorithm was used to correct for background signal resulting from the LSO intrinsic radiation, since the TOF reconstruction sufficiently removes the LSO coincidence events from the rhesus monkey volume.

Regions-of-interest (ROIs) were manually extracted from the reconstructed PET images at each time-point and used to quantify the mean activity concentration in the liver, kidney, blood (mediastinal blood pool), bone (shoulders and pelvis), as well as the total activity in the body. Activity distributions in each ROI were quantified using standard uptake value (SUV):

$$SUV = \frac{\overline{c_{img}}}{ID/m} \quad (1)$$

where $\overline{c_{img}}$ is the mean activity concentration in the ROI, ID is the total injected dose on day 0, and m is the mass of the animal.

RESULTS

Image Quality

Reconstructed PET images of a single rhesus monkey at all imaging time-points are shown in Fig. 1. Importantly for this study, the image quality obtained at late time-points (days 7 to 30); even at 30-days post-injection, with an absolute residual whole-body activity of less than 40 kBq, was sufficient to identify ^{89}Zr signal in the liver, kidneys, and several sites of uptake at bone epiphyses (shoulder, pelvis, knee). Additionally, excellent image quality was achieved at early time-points, clearly capturing the initial antibody distribution throughout the body.

Day 0 Pharmacokinetics

A comparison of early kinetics is demonstrated in Fig. 2, showing the dynamic series of images acquired on day 0 from one rhesus monkey in each chelator-linker group (subjects "B", see Table 1). As expected for intact antibodies, there is little change in the ^{89}Zr-antibody biodistribution in the first hour post-injection due to the slow extraction rate of antibodies from the bloodstream. The behavior observed in the first hour is potentially informative regarding the presence and nature of unwanted low molecular weight impurities or degradation products in the sample for injection.

Two important differences in the early pharmacokinetics likely related to clearance routes are noted. First, both Bz-NCS linker groups show increasing activity in the bladder towards the end of the 60-minute scan (yellow arrows), whereas both squaramide linker groups showed very little bladder activity. The bladder activity measured from the last 10-minute frame was quantified for all subjects in Fig. 3 and showed close agreement with the image assessment. Importantly, high bladder activity for the Bz-NCS linker groups may indicate the presence of low molecular weight ^{89}Zr-DFO or ^{89}Zr-DFO* complexes, which are known to be rapidly cleared via the renal system (*27,28*). The QC purity measurements (Supplemental Figs. 2C and 2D) indicate negligible (<5%) impurities in the squaramide groups out to three-days post-synthesis, which is reflected in the

negligible renal clearance in these groups. The Bz-NCS groups (Supplemental Figs 2A and 2B), on the other hand, exhibited progressively increased low molecular weight impurities consistent with unbound ^{89}Zr-DFO-Bz-NCS and ^{89}Zr-DFO*-Bz-NCS and the high bladder activity. However, while the imaging suggests greater impurity levels in the ^{89}Zr-DFO-Bz-NCS material, the QC data showed the opposite: the ^{89}Zr-DFO*-Bz-NCS QC data indicated approximately 3% and 25% impurities at 0 and five days post-synthesis respectively, while the ^{89}Zr-DFO-Bz-NCS QC data showed approximately 6% and 17% impurities at 0 and three days post-synthesis, respectively. These results cannot be entirely reconciled since the imaging and QC samples were separated and handled somewhat differently, with potential for exposure to different conditions of temperature and agitation on the day of transport, for example.

Second, there is an interesting increase in activity in the gastrointestinal (GI) tract that was observed in all animals within the DFO-Bz-NCS group (red arrow), but not observed in any animal within the other three chelator-linker groups. Increased GI uptake likely represents hepatobiliary clearance of hydrophobic impurities, and possibly some fraction of the low molecular weight forms of the ^{89}Zr-DFO-linker.

Late Time-Point Pharmacokinetics

Images acquired at ~14 days post-injection (DFO*-Bz-NCS group acquired day 17) for all rhesus monkeys are shown in Fig. 4. Within each chelator-linker group there is little visual variability in the activity biodistributions, while easily identifiable differences in activity concentration, for example in the liver, bone, and whole-body, are observed across the four groups.

Time activity curves with mean SUV in the liver, kidneys, bone, blood, and whole-body activity at each imaging time-point are shown in Fig. 5 for all animals. As suggested from the day 14 image comparisons (Fig. 4), significant differences in uptake in several organs and tissues were measured

at late time-points across the four chelator-linker groups. Within each chelator-linker group, however, there was little variation in the pharmacokinetics for all anatomical sites measured.

The main outlying data appears in the day 0 blood activity measurements, where there are large differences in the measured blood activity concentrations across the three animals/group within some of the chelator-linker groups (e.g., DFO-Bz-NCS). This contrasts the consistent whole-body activity values and ELISA data. Upon inspection, it was found that for some of the animals, a fraction of activity remained at the injection site on day 0 and may explain the reason for some outlier blood activity values on day 0. For example, two of the animals in the DFO-Bz-NCS group (circle and triangle markers) were found to have ~4 MBq and ~12.4 MBq activity, respectively, residing at the injection site at the end of the day 0 scan.

Although there is good agreement between the image-derived blood activity concentration and the ELISA data at later time-points, there appear to be some inconsistencies at the earliest time-point, primarily with the DFO-Bz-NCS group. In this group, the image-derived blood activity shows a decline between day 0 and day two compared to the other three chelator-linker groups, while the ELISA data is largely consistent across all four groups. This is presumably related to the presence of low molecular weight impurities that is also suggested by the high bladder clearance on day 0. Additionally, some of the inconsistencies between the image-derived blood activity and the ELISA measurements may be influenced by a fraction of radioactivity (versus total antibody) at the injection site.

DISCUSSION

In these studies, we demonstrated the feasibility of 30-day duration ^{89}Zr PET imaging studies in rhesus monkeys, enabled through the use of the high sensitivity primate mini-EXPLORER total-body PET system. Sufficient image quality was maintained throughout the 30-day study period, a duration equivalent to approximately nine radioactive half-lives of ^{89}Zr, and used to quantify

antibody uptake in the liver, kidneys, blood, bone (shoulder), and whole-body activity. Quantitative image analysis revealed potentially important differences in the 30-day pharmacokinetics associated with four different ^{89}Zr chelator-linker combinations and their (implied) catabolites. Comparisons with ELISA outcomes showed that the circulating ^{89}Zr in the plasma mostly remained bound to antibody throughout the experiment, especially once initial low molecular weight impurities were discounted, which was an essential step for interpreting DFO-Bz-NCS results (Supplemental Fig. 3).

The study was not designed to suggest optimal formulation conditions for the radiolabeled antibodies used, rather the formulation employed was at the time of the study considered reliable having been used for commercial therapeutic antibody products and for many small-scale (~MBq labeling) antibody-PET studies. We were surprised to find high levels of low molecular weight impurities formed over time and contained in the injected material in the Bz-NCS linker groups. Consequently, we note the importance of optimizing formulations for shelf-life stability using labeling, shipping, and QC studies on the same scale as the imaging production runs. Multi-day shelf-life stability is a necessary pre-requisite to enable distributed use of ^{89}Zr tracers, and will be important for human clinical studies.

Interestingly, the octadentate DFO*-squaramide and DFO*-Bz-NCS reagents were noted with markedly less conspicuous uptake at the bone joints than DFO-squaramide (p-value < 0.05 for all time-points after day 0). This may be important to reduce sites of focal uptake that could complicate image interpretation, and perhaps pose a risk of non-specific signal arising at sites of injury or remodeling associated with metastatic disease.

Conversely, the DFO-squaramide reagent showed substantial conspicuous bone uptake, approximately three to four-fold higher compared to all three other chelator-linker groups at

imaging time-points later than seven days post-injection, suggesting that this octadentate ligand was not as beneficial to the osteophilic properties of ^{89}Zr catabolites as the DFO*. It should be noted that even the high bone uptake within the DFO-squaramide group measured in rhesus monkeys is much lower than the values reported in young mice and rats, which has been shown in mice to be as high as 10-15% of the injected dose at time-points later than three days post-injection (*29*).

The DFO-squaramide was also unusual in that, at the end of the 30-day study period, less than 50% of the ^{89}Zr was cleared from body in all three animals per group even though the ELISA showed that the antibody was clearing from the circulation similarly across groups.

Overall, the impurity QC measurements were good predictors of early bladder activity, except for the DFO-Bz-NCS group. This mismatch likely involved greater radiolytic degradation in the sample of ^{89}Zr-labeled antibody transported to the imaging suite without temperature control than the better-controlled sample retained for the QC testing.

The other major difference between the chelator-linker groups that relates to elimination was observed in the whole-body measurements and perhaps dominated by the measured liver uptake. Here the DFO-squaramide group showed substantially higher liver uptake compared to the other groups (p-value < 0.02 for all time-points after day 0). The liver showed uptake because it is a site for antibody catabolism as well as the clearance route for many small molecules, protein and cell aggregates, and colloids such as zirconium-phosphate (*29*). However, the identification of the form of ^{89}Zr-DFO-squaramide persisting in the liver would have required biopsies which were not performed in this study.

Further investigations could address additional parameters. In particular, we did not include DFO-N-Suc-TFP, perhaps considered the reagent most widely used for clinical antibody-PET

studies to date. Our priority was to compare DFO and DFO* on the same Bz-NCS linker system, and to study the properties of the promising squaramide linker. Future approaches could also address important aspects of the chelator reagents used such as solubility and behavior in the conjugation process, which might be compared when selecting a chelator-linker combination for antibody-PET or similar ^{89}Zr studies. Further work is underway to more fully characterize the various reagents in these terms, and to compare their chemical and imaging properties as they relate to tumor and bone uptake in more detail.

Overall, these results suggest that the use of octadentate DFO* gives rise to fewer osteophilic catabolites and a better late time-point image signal, presumably the result of a more stable bond complex with ^{89}Zr compared to hexadentate DFO. The squaramide linker may also provide some advantages in shelf-life stability when compared to Bz-NCS.

CONCLUSION

The feasibility of extending ^{89}Zr-PET studies for 30-days post-injection was demonstrated in these studies using the high sensitivity primate mini-EXPLORER PET system. Using a cohort of 12 young rhesus monkeys, the pharmacokinetics associated with four ^{89}Zr chelator-linkers were evaluated in combination with humanized IgG antibodies. Quantitative image analysis suggests that using the octadentate chelator DFO* results in improved ^{89}Zr chelating stability, as evidenced by differences in bone and liver uptake at the later time-points. Overall, excellent consistency was observed within each group even at very late time-points, and which enabled the observation of interesting differences in tissue and bone uptake with the various chelators and linkers. The results also suggest that careful selection of reagents and rigorous assessment of shelf-life stability is warranted for future studies.

DISCLOSURE

We acknowledge support from NIH R35-CA197608 and P51-OD011107. No other potential conflicts of interest relevant to the article exist.

ACKNOWLEDGEMENTS

The authors would like to thank the Center for Molecular and Genomic Imaging for assistance and the staff of the Primate Center Multimodal Imaging Core.

KEY POINTS

QUESTION: Is quantitative ^{89}Zr-antibody-PET imaging feasible up to 30-days post-injection, and if so, what is the *in vivo* behavior of several common DFO-variant chelators over this duration?

PERTINENT FINDINGS: Accurate quantification indicated by highly consistent pharmacokinetics within each chelator-linker group was maintained over the 30-day study duration owing to the high sensitivity of the long axial field-of-view PET system. Significant differences were observed in the pharmacokinetics associated with each chelator-linker moiety, attributed to both differences in *in vivo* behavior as well as shelf-life stability.

IMPLICATIONS FOR PATIENT CARE: The feasibility of long duration ^{89}Zr imaging with total-body PET enables physiologically optimized imaging time-points that are not limited by scanner sensitivity. The chelator pharmacokinetics comparison is a necessary pre-requisite to enable distributed use of ^{89}Zr tracers for human clinical studies.

REFERENCES

1. Berg E, Zhang X, Bec J, et al. Development and evaluation of mini-EXPLORER: a long axial field-of-view PET scanner for non-human primate imaging. *J Nucl Med.* 2018;59:993-998

2. Lyu Y, Lv X, Liu W, et al: Mini EXPLORER II: a prototype high-sensitivity PET/CT scanner for companion animal whole body and human brain scanning. *Phys Med Biol.* 2019;64:075004

3. Badawi RD, Shi H, Hu P, et al. First human imaging studies with the EXPLORER total-body PET scanner. *J Nucl Med.* 2019;60:299-303

4. Karp J, Schmall J, Geagan M, et al. Imaging Performance of the PennPET Explorer scanner. *J Nucl Med.* 2018;59(S1):222

5. Cherry SR, Jones T, Karp JS, et al. Total-body PET: Maximizing sensitivity to create new opportunities for clinical research and patient care. *J Nucl Med.* 2018;59:3-12

6. van Dongen GA, Visser GW, Lub-de Hooge MN, et al. Immuno-PET: a navigator in monoclonal antibody development and applications. *Oncologist.* 2007;12:1379-1389

7. van Dongen GA, Vosjan MJ. Immuno-positron emission tomography: shedding light on clinical antibody therapy. *Cancer Biother Radiopharm.* 2010;25:375-385

8. Vugts DJ, Visser GW, van Dongen GA. 89Zr-PET radiochemistry in the development and application of therapeutic monoclonal antibodies and other biologicals. *Curr Top Med Chem.* 2013;13:446-457

9. Tarantal AF, Lee CCI, Kukis DL, et al. Radiolabeling human peripheral blood stem cells for positron emission tomography (PET) imaging in young rhesus monkeys. *PloS One.* 2013;8:e77148

10. Sato N, Wu H, Asiedu KO, et al. 89Zr-oxine complex PET cell imaging in monitoring cell-based therapies. *Radiology*. 2015;275:490-500

11. Keliher EJ, Yoo J, Nahrendorf M, et al. 89Zr-labeled dextran nanoparticles allow in vivo macrophage imaging. *Bioconj Chem.* 2011;22:2383-2389

12. Ruggiero A, Villa CH, Holland JP, et al. Imaging and treating tumor vasculature with targeted radiolabeled carbon nanotubes. *Int J Nanomedicine*. 2010;5:783-802

13. Deri MA, Zeglis BM, Francesconi LC, et al. PET imaging with 89Zr: from radiochemistry to the clinic. *Nucl Med Biol.* 2013;40:3-14

14. Fischer G, Seibold U, Schirrmacher R, et al. 89Zr, a radiometal nuclide with high potential for molecular imaging with PET: chemistry, applications and remaining challenges. *Molecules.* 2013;18:6469-6490

15. Bansal A, Pandey MK, Demirhan YE, et al. Novel 89 Zr cell labeling approach for PET-based cell trafficking studies. *EJNMMI Res.* 2015;5:19

16. Ulaner GA, Hyman DM, Ross DS, et al. Detection of HER2-positive metastases in patients with HER2-negative primary breast cancer using 89Zr-trastuzumab PET/CT. *J Nucl Med*. 2016;57:1523-1528

17. Bhatt N, Pandya D, Wadas T. Recent advances in zirconium-89 chelator development. *Molecules.* 2018;23:638

18. Perk LR, Vosjan MJ, Visser GW, et al. p-Isothiocyanatobenzyl-desferrioxamine: a new bifunctional chelate for facile radiolabeling of monoclonal antibodies with zirconium-89 for immuno-PET imaging. *EJNMMI.* 2010;37:250-259

19. Verel I, Visser GW, Boellaard R, et al. 89Zr immuno-PET: comprehensive procedures for the production of 89Zr-labeled monoclonal antibodies. *J Nucl Med.* 2003;44:1271-1281

20. Dijkers E, Munnink TO, Kosterink J, et al. Biodistribution of 89Zr-trastuzumab and PET imaging of HER2-positive lesions in patients with metastatic breast cancer. *Clin Pharmacol Ther.* 2010;87:586-592

21. Holland JP, Evans MJ, Rice SL, et al. Annotating MYC status with 89 Zr-transferrin imaging. *Nat Med.* 2012;18:1586

22. Vugts DJ, Klaver C, Sewing C, et al. Comparison of the octadentate bifunctional chelator DFO*-pPhe-NCS and the clinically used hexadentate bifunctional chelator DFO-pPhe-NCS for 89 Zr-immuno-PET. *EJNMMI.* 2017;44:286-295

23. Patra M, Bauman A, Mari C, et al. An octadentate bifunctional chelating agent for the development of stable zirconium-89 based molecular imaging probes. *Chem Comm.* 2014;50:11523-11525

24. Rudd SE, Roselt P, Cullinane C, et al. A desferrioxamine B squaramide ester for the incorporation of zirconium-89 into antibodies. *Chem Comm.* 2016;52:11889-11892

25. Vosjan MJ, Perk LR, Visser GW, et al. Conjugation and radiolabeling of monoclonal antibodies with zirconium-89 for PET imaging using the bifunctional chelate p-isothiocyanatobenzyl-desferrioxamine:.*Nat Prot.* 2010;5:739

26. Carney JP, Townsend DW, Rappoport V, et al. Method for transforming CT images for attenuation correction in PET/CT imaging. *Med Phys.* 2006;33:976-983

27. Abou DS, Ku T, Smith-Jones PM. In vivo biodistribution and accumulation of 89Zr in mice. *Nucl Med Biol.* 2011;38:675-681

28. Meijs WE, Haisma HJ, Van Der Schors R, et al. A facile method for the labeling of proteins with zirconium isotopes. *Nucl Med Biol.* 1996;23:439-448

29. Holland JP, Divilov V, Bander NH, et al. 89Zr-DFO-J591 for immunoPET imaging of prostate-specific membrane antigen (PSMA) expression in vivo. *J Nucl Med.* 2010;51:1293-1300

FIGURES

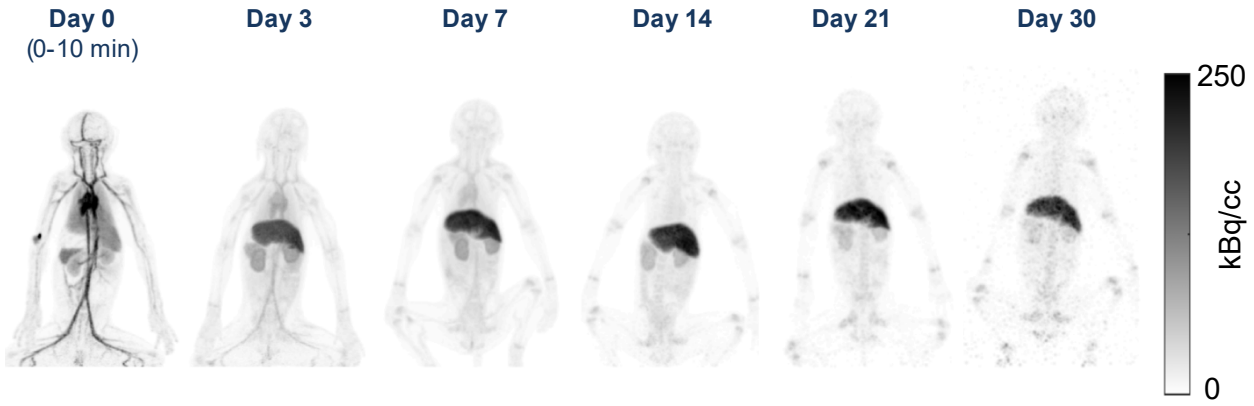

FIGURE 1. Maximum intensity projection images at each time point for one of the rhesus monkeys in the ^{89}Zr-DFO-squaramide-anti-gD group. All images use the same grayscale range of 0-250 kBq/cc.

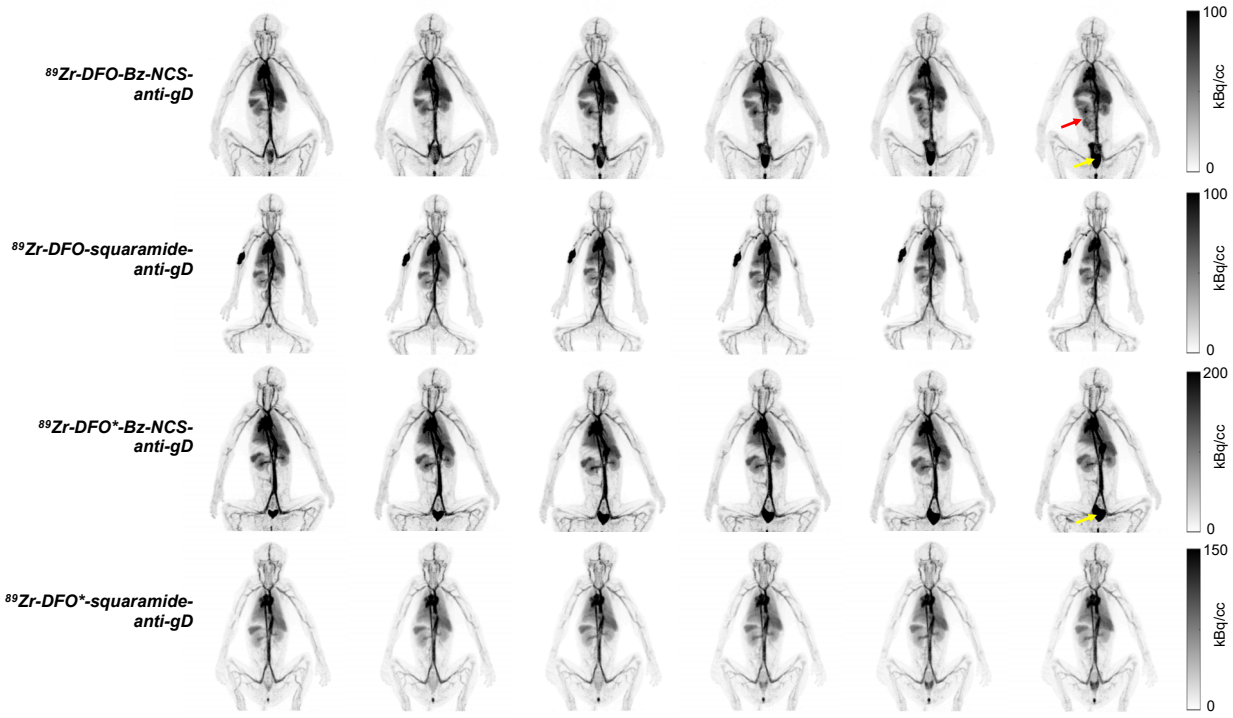

FIGURE 2. Dynamic image sequence acquired on day 0 for rhesus monkey 'B' in each of the chelator-linker groups. Each image is 10-minute duration, with the first image beginning approximately three minutes after the antibody injections. The hot spot in the arm of the ^{89}Zr-DFO-squaramide-anti-gD group represents activity at the injection site. Yellow arrows indicate activity in the bladder observed in the ^{89}Zr-DFO-Bz-NCS-anti-gD and ^{89}Zr-DFO*-Bz-NCS-anti-gD groups. The red arrow indicates activity in the GI tract observed only in the ^{89}Zr-DFO-Bz-NCS-anti-gD group.

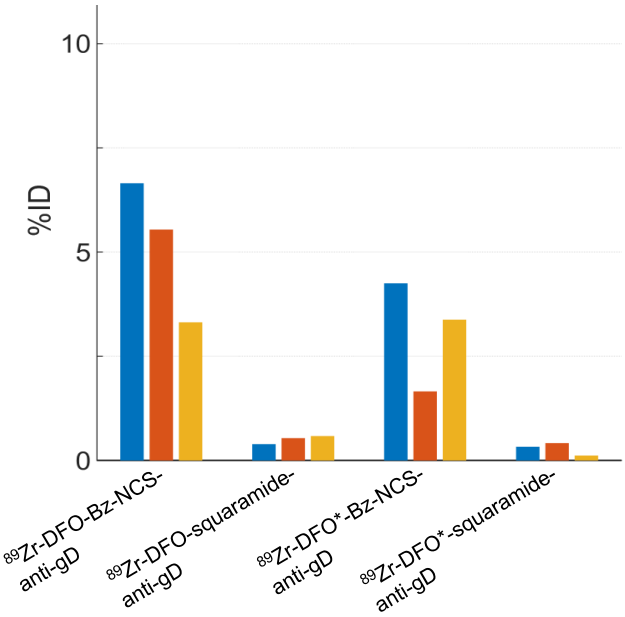

FIGURE 3. Bladder activity measured in the last 10-minute frame on day 0, approximately 50-60 minutes post-injection. Each bar represents one rhesus monkey. %ID: percent injected dose.

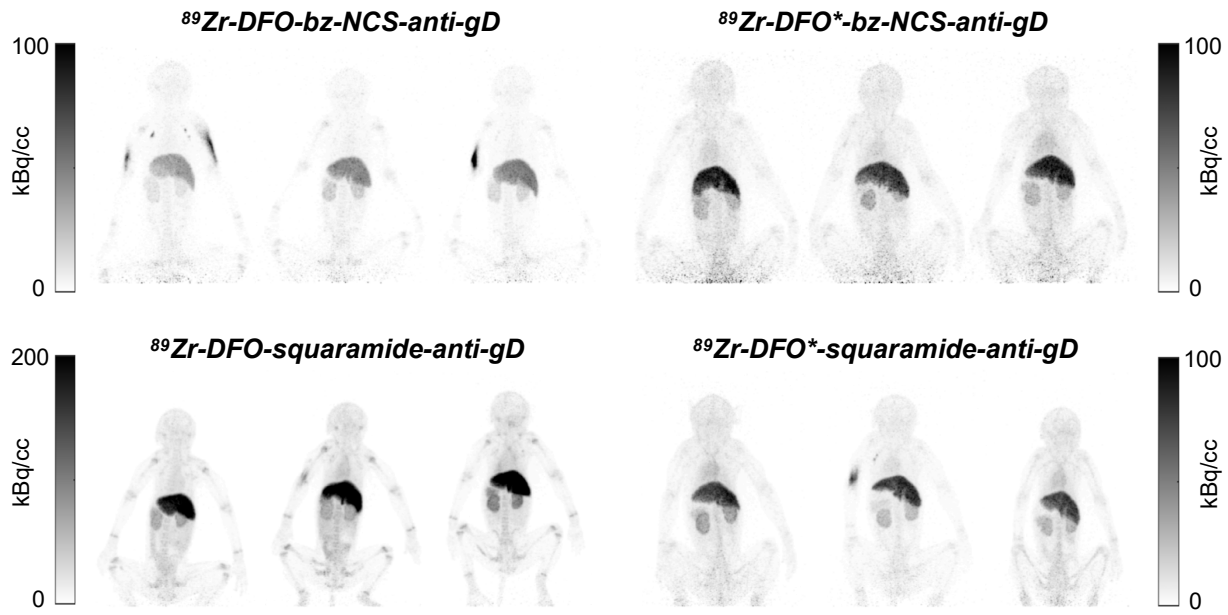

FIGURE 4. Maximum intensity projection PET images acquired on day 14 for all animals. Overall, there is excellent consistency in whole-body activity and uptake in easily identifiable organs and tissues, while differences are noted across the groups. Note the different grayscale used for the ^{89}Zr-DFO-squaramide-anti-gD group. The hot spots in the arm of some rhesus monkeys represent residual activity at the injection site from day 0. The animal order (left to right) for each group is A, B, and C (see Table 1).

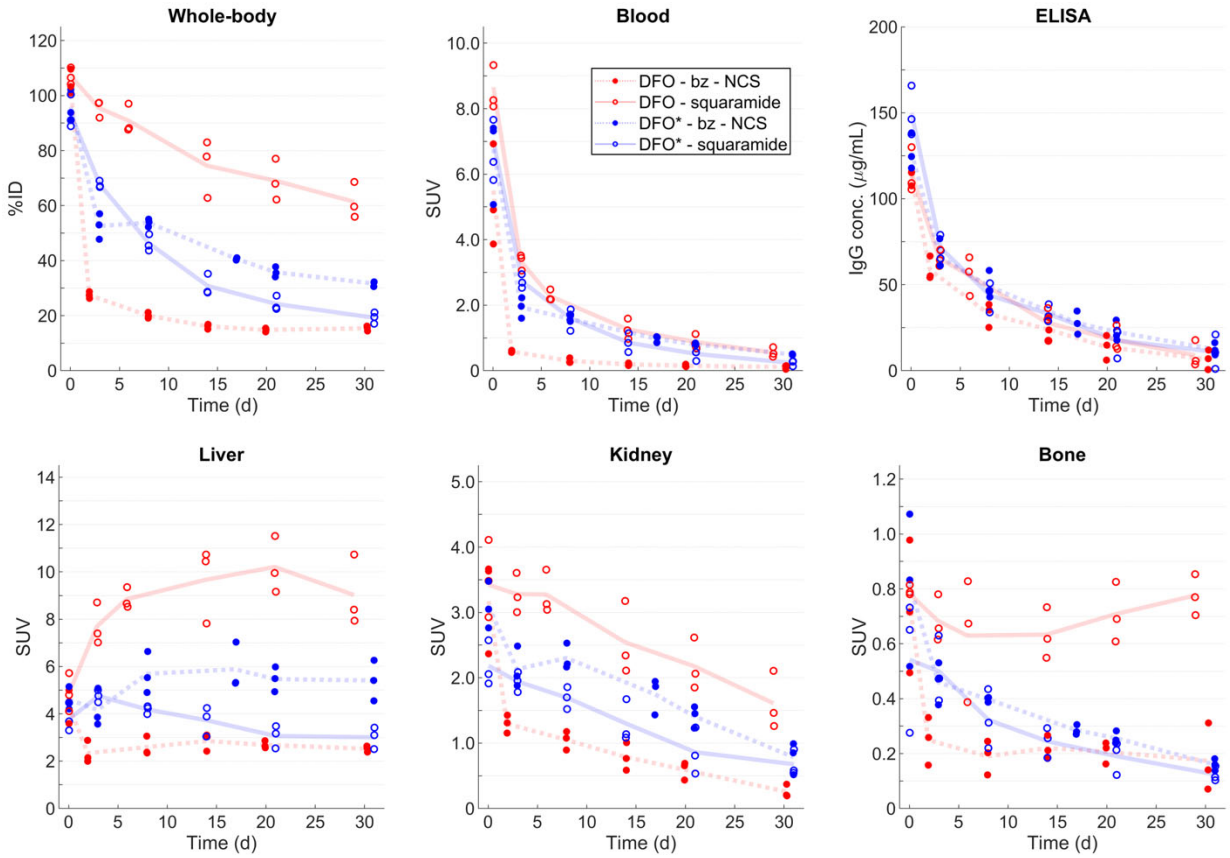

FIGURE 5. Time-activity curves for each ROI. The markers indicate measurements for each animal, while the lines represent the mean value for each chelator-linker group. All figures use the same legend as indicated. The whole-body activity was normalized to the injected dose for each subject (ID: injected dose).

TABLES

TABLE 1. Experimental design.

Group	Monkey subject ID	Weight (kg)	Age (years)	Injected ^{89}Zr dose (MBq)	Imaging time-points (days post-injection)
^{89}Zr-DFO-Bz-NCS-anti-gD	A	2.87	1.2	37.4	0, 2, 7, 14, 20, 30
	B	2.87	1.2	36.2	
	C	3.55	1.5	38.8	
^{89}Zr-DFO*-Bz-NCS-anti-gD	A	3.16	1.5	39.5	0, 3, 7, 17, 21, 31
	B	3.35	1.8	36.6	
	C	3.77	2.0	37.4	
^{89}Zr-DFO-squaramide-anti-gD	A	1.75	1.0	42.0	0, 3, 6, 14, 21, 29
	B	1.92	1.0	42.4	
	C	2.24	1.0	43.6	
^{89}Zr-DFO*-squaramide-anti-gD	A	3.00	1.3	47.1	0, 3, 7, 14, 21, 31
	B	2.62	1.2	40.7	
	C	2.25	1.2	41.8	

DFO-Bz-NCS-anti-gD

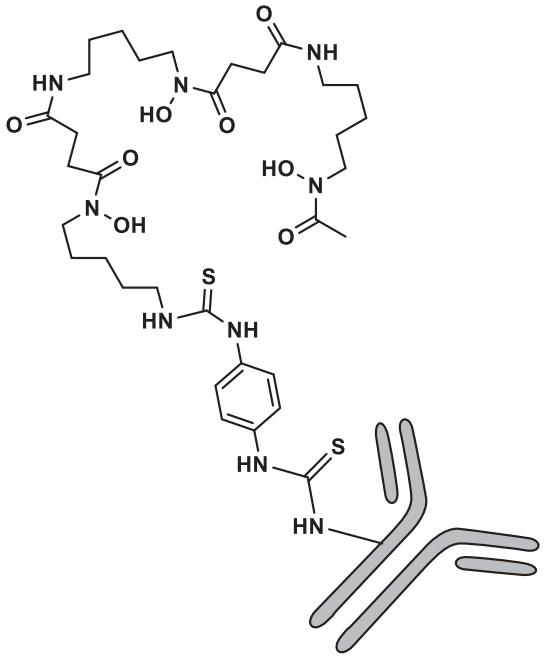

DFO*-Bz-NCS-anti-gD

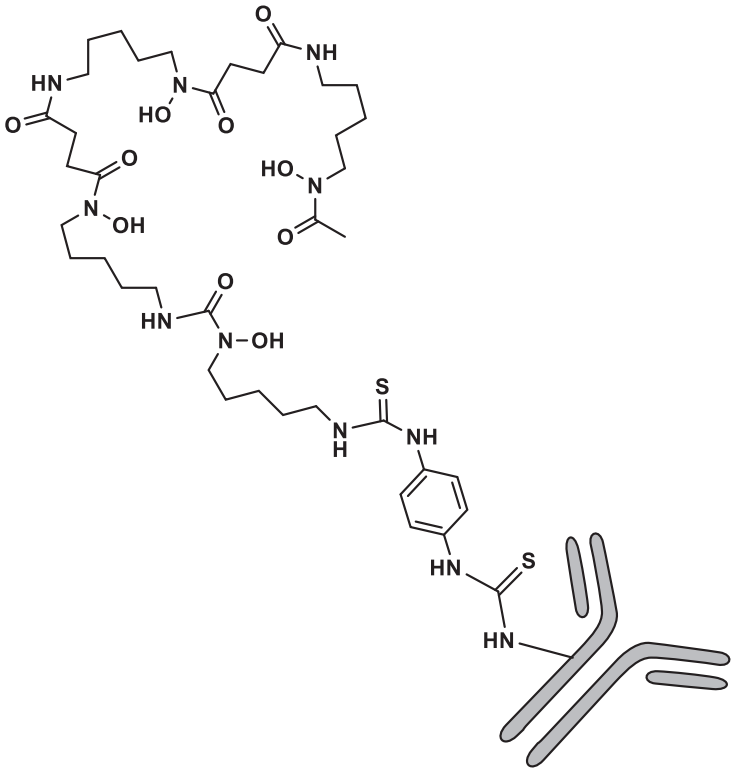

DFO-squaramide-anti-gD

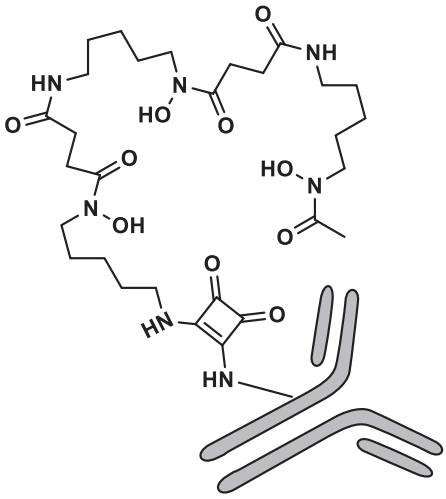

DFO*-squaramide-anti-gD

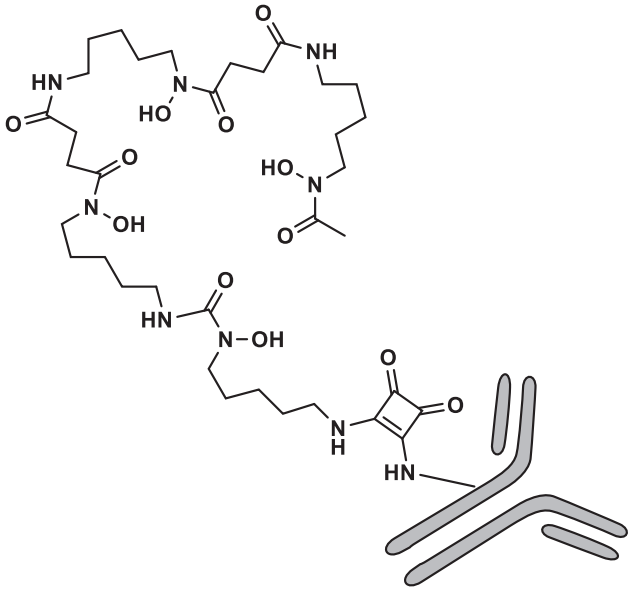

Supplemental Figure 1. Chemical structures of the four chelator-linker combinations investigated in this study. (Courtesy of Lan Na, Chemistry, UC Davis).

^{89}Zr-DFO-bz-NCS-anti-gD mAb

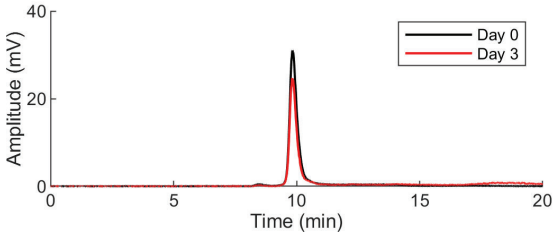

Day 0: 2.0% aggregates, 93.7% monomer, 2.3% free ^{89}Zr, 2.0% peak at 17-19 min (presumed to be ^{89}Zr-DFO-bz-NCS analog)

Day 3: 1.0% aggregates, 83.3% monomer, 15.7% peak at 17-19 min (presumed to be ^{89}Zr-DFO-bz-NCS analog)

^{89}Zr-DFO-squaramide-anti-gD mAb

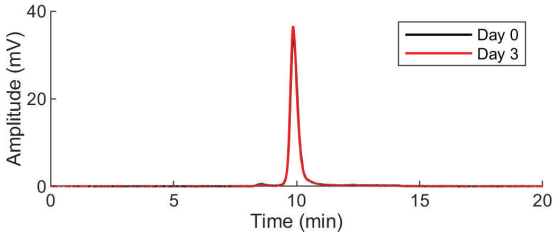

Day 0: 1.9% aggregates, 96.6% monomer, 1.5% free ^{89}Zr

Day 3: 1.3% aggregates, 97.4% monomer, 1.3% free ^{89}Zr

^{89}Zr-DFOstar-bz-NCS-anti-gD mAb

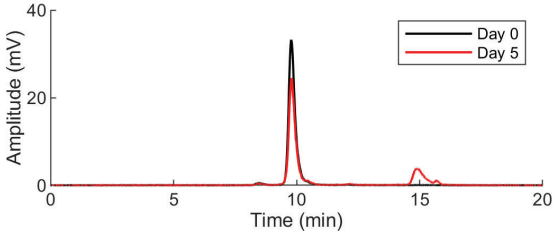

Day 0: 2.0% aggregates, 97.1% monomer, 0.4% free ^{89}Zr, 0.5% ^{89}Zr-DFO*

Day 5: 1.3% aggregates, 75.2% monomer, 0.5% mAb fragments, 1.5% free ^{89}Zr; 21.5% ^{89}Zr-DFO*

^{89}Zr-DFO*-squaramide-anti-gD mAb

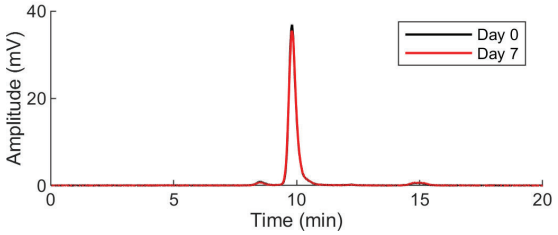

Day 0: 3.0% aggregates, 93.5% monomer, 0.6% free ^{89}Zr, 2.9% peak at ~15 min (presumed to be ^{89}Zr-DFO*-squaramide analog)

Day 7: 2.6% aggregates, 90.7% monomer, 1.1% free ^{89}Zr, 5.5% peak at ~15 min (presumed to be ^{89}Zr-DFO*-squaramide analog)

Supplemental Figure 2. Chemical purities of each chelator-linker measured by size-exclusion HPLC (System C in the text).

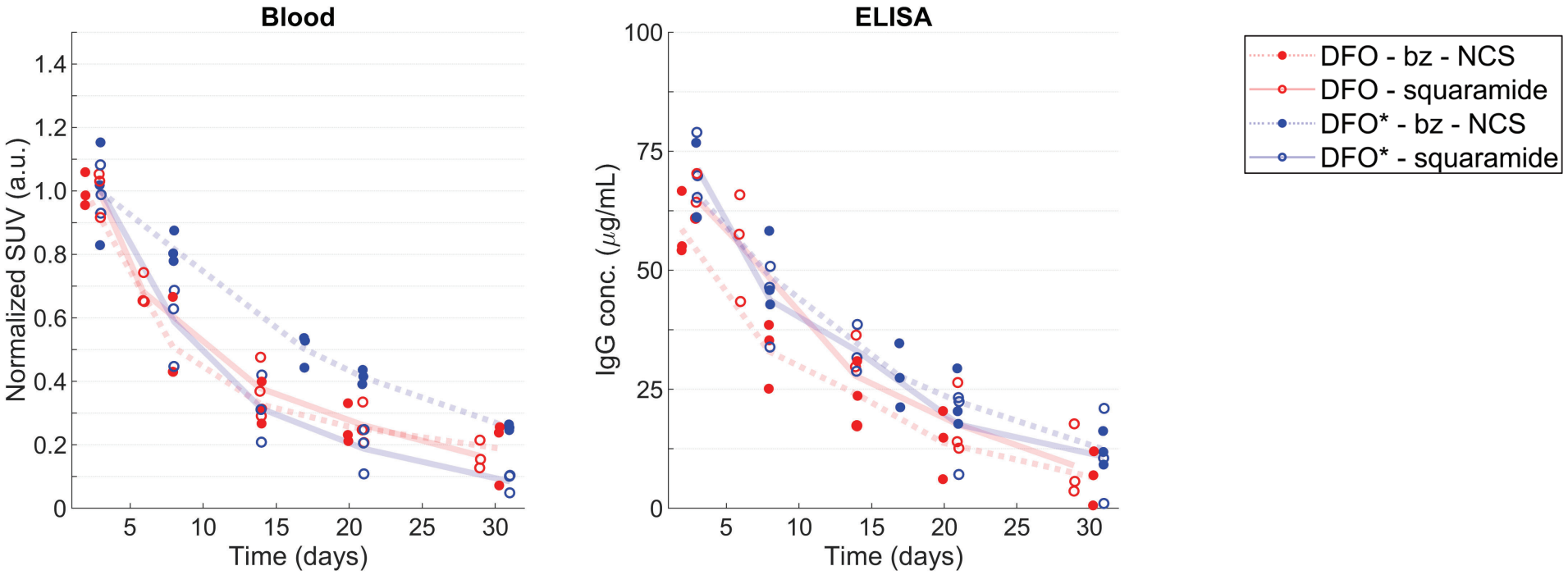

Supplemental Figure 3. Comparison of blood SUV and ELISA antibody concentration for days 2 – 30. The blood SUV for each group are normalized by the mean value on day 2/3.